The Astronomical Journal, 131:2643–2651, 2006 May

NRL Release Number 06-1226-4270

THE HYADES BINARY θ^2 TAURI: CONFRONTING EVOLUTIONARY MODELS WITH OPTICAL INTERFEROMETRY

J. T. Armstrong
Remote Sensing Division, Naval Research Laboratory, Code 7215,
Washington, DC 20375; tom.armstrong@nrl.navy.mil

D. Mozurkewich
Seabrook Engineering, 9310 Dubarry Avenue, Seabrook, MD 20706; dave@mozurkewich.com

Arsen R. Hajian and K. J. Johnston
US Naval Observatory, 3450 Massachusetts Avenue NW, Washington, DC 20392-5420;
hajian.arsen@usno.navy.mil, kjj@astro.usno.navy.mil

R. N. Thessin
C. S. Draper Laboratory, Massachusetts Institute of Technology, 555 Technology Square, MS 84,
Cambridge, MA 02139; rthessin@mit.edu

Deane M. Peterson
Astronomy Program, State University of New York, Stony Brook, NY 11794-2100; dpeterson@astro.sunysb.edu

C. A. Hummel
European Southern Observatory, Casilla 19001, Santiago 19, Chile; chummel@eso.org

and

G. C. Gilbreath
Remote Sensing Division, Naval Research Laboratory, Code 7215, Washington, DC 20375; gilbreath@nrl.navy.mil
Received 2005 February 23; accepted 2006 January 12

ABSTRACT

We determine the masses and magnitude difference of the components of the Hyades spectroscopic binary θ^2 Tauri. We find that both components appear to be less massive and/or brighter than predicted from some recent evolutionary models. The rapid rotation and unknown rotational inclination of both components introduce uncertainty in their luminosities and colors, but not enough to reconcile both of them with the evolutionary models. We measured the visual orbit with the Mark III optical interferometer and the Navy Prototype Optical Interferometer and combined it with the *Hipparcos* proper-motion-based parallax to find a total system mass $\Sigma\mathcal{M}$ of $4.03 \pm 0.20\ \mathcal{M}_{\odot}$. We also combined our visual orbit with three recent spectroscopic orbits to find three spectroscopically based estimates of $\Sigma\mathcal{M}$ and compared these to the $\Sigma\mathcal{M}$ from the visual orbit and parallax. We chose the spectroscopic orbit that agreed best and used its mass ratio to estimate individual masses $\mathcal{M}_{\mathrm{A,B}}$ of 2.15 ± 0.12 and $1.87 \pm 0.11\ \mathcal{M}_{\odot}$. From the interferometry, we determine $\Delta m = 1.13 \pm 0.05$ mag across the 450–850 nm band. The parallax then implies absolute V magnitudes $M_{\mathrm{A,B}}$ of 0.48 ± 0.05 and 1.61 ± 0.06 mag. If the components are rotating near breakup velocity and seen nearly pole-on, the true luminosities may be as faint as 1.03 and 2.13 mag; even in that case, however, the secondary is too blue by $\sim$0.07 mag in $B - V$.

Key words: binaries: spectroscopic — binaries: visual — stars: individual (θ^2 Tauri) — techniques: interferometric

Online material: OIFITS file

1. INTRODUCTION

The binary θ^2 Tauri, the brightest member of the Hyades, excited some interest in the 1990s as the 19 mas visual orbit was resolved by interferometry (Armstrong et al. 1991; Pan et al. 1992; Hummel & Armstrong 1992), while the spectral lines of the rapidly rotating secondary were disentangled from those of the primary (also a rapid rotator) to yield a double-lined spectroscopic orbit by Peterson (1991, hereafter P91), Peterson et al. (1993, hereafter PSL93), Tomkin et al. (1995, hereafter TPM95), and Torres et al. (1997, hereafter TSL97). In the early 1990s, the lure of θ^2 Tau was the orbital parallax—and thus the distance to the Hyades—to be derived from the visual and spectroscopic elements.

By the late 1990s, the *Hipparcos* trigonometric parallax was available (Perryman et al. 1998), with precision comparable to or better than that of the orbital parallax. In 2001, de Bruijne et al. published an even more precise proper-motion-based parallax of θ^2 Tau in the process of evaluating the parallaxes of a large number of Hyades members and determining the distance to the cluster. As a result, θ^2 Tau is now interesting not so much for its distance as for the constraints that the masses and luminosities of its components impose on the evolutionary state and elemental abundances of the Hyades. In particular, its components, along with 51 Tau A, are the only Hyades stars near the turnoff point with measured masses.

The problems with using the masses of θ^2 Tau currently in the literature are that the visual orbit, based on data from the Mark III optical interferometer, has been reported only in preliminary versions, while there are not one, but three, recent spectroscopic orbit calculations with somewhat discordant results. The spectroscopic results and the implied masses, distances, and magnitudes

Report Documentation Page

Form Approved
OMB No. 0704-0188

1. REPORT DATE	2. REPORT TYPE	3. DATES COVERED
MAY 2006		**00-00-2006 to 00-00-2006**

4. TITLE AND SUBTITLE	5a. CONTRACT NUMBER
The Hyades Binary 2 Tauri: Confronting Evolutionary Models with Optical Interferometry	5b. GRANT NUMBER
	5c. PROGRAM ELEMENT NUMBER
6. AUTHOR(S)	5d. PROJECT NUMBER
	5e. TASK NUMBER
	5f. WORK UNIT NUMBER
7. PERFORMING ORGANIZATION NAME(S) AND ADDRESS(ES) **Naval Research Laboratory,Code 7215,4555 Overlook Avenue SW,Washington,DC,20375**	8. PERFORMING ORGANIZATION REPORT NUMBER
9. SPONSORING/MONITORING AGENCY NAME(S) AND ADDRESS(ES)	10. SPONSOR/MONITOR'S ACRONYM(S)
	11. SPONSOR/MONITOR'S REPORT NUMBER(S)

12. DISTRIBUTION/AVAILABILITY STATEMENT
Approved for public release; distribution unlimited

13. SUPPLEMENTARY NOTES

14. ABSTRACT
see report

15. SUBJECT TERMS

16. SECURITY CLASSIFICATION OF:			17. LIMITATION OF ABSTRACT	18. NUMBER OF PAGES	19a. NAME OF RESPONSIBLE PERSON
a. REPORT **unclassified**	b. ABSTRACT **unclassified**	c. THIS PAGE **unclassified**	**Same as Report (SAR)**	**9**	

TABLE 1
Recent Spectroscopic Results

Parameter	PSL93/P91[a]	TPM95[b]	TSL97[b]
Spectroscopy			
K_A (km s^{-1})	31.2 ± 0.9	29.3 ± 0.3	33.18 ± 0.39
K_B (km s^{-1})	42.7 ± 2.4	38.0 ± 2.8	38 ± 2
$v_A \sin i$ (km s^{-1})	65	70 ± 5	70
$v_B \sin i$ (km s^{-1})	170	90 ± 20	110 ± 4
q	0.73 ± 0.05	0.77 ± 0.06	0.873 ± 0.048
With Visual Elements Added			
ϖ_{orb} (mas)	21.86 ± 0.90	22.7 ± 1.1	21.22 ± 0.76
D (pc)	45.7 ± 1.9	44.1 ± 2.2	47.10 ± 1.7
$m - M$ (mag)	3.302 ± 0.089	...	3.37 ± 0.08
$\mathcal{M}_A$ ($\mathcal{M}_\odot$)	2.48 ± 0.37	2.1 ± 0.3	2.42 ± 0.30
$\mathcal{M}_B$ ($\mathcal{M}_\odot$)	1.80 ± 0.17	1.6 ± 0.2	2.11 ± 0.17

[a] As calculated from PSL93 using correct Δv_R data from P91 (see text) and visual orbital elements from this work.
[b] As published by TPM95 and TSL97 using visual orbital elements from Pan et al. (1992).

are summarized in Table 1 (with corrections to the PSL93 results; see § 2.1). The de Bruijne et al. (2001) parallax and the visual interferometric orbit we present here significantly clarify the situation, as we show below.

Our visual orbit is based on 30 nights of data from the Mark III optical interferometer,[1] which ceased operations at the end of 1992, and four nights of data from the Navy Prototype Optical Interferometer[2] (NPOI), which has operated at the Lowell Observatory site on Anderson Mesa, Arizona, since 1995. The NPOI data improve the sampling near periastron and include closure phases, which permit us to resolve the 180° ambiguity in the position angle of the line of nodes. The resulting orbit is consistent with, but considerably more precise than, the preliminary orbits published by Armstrong et al. (1991), Pan et al. (1992), and Hummel & Armstrong (1992) based on subsets of the Mark III data.

Besides presenting the visual orbit, the purpose of this paper is to infer the best component-mass estimates by combining the best spectroscopic orbit with our visual orbit. To select the best spectroscopic orbit, we first use the fact that the total system mass can be determined by combining the visual orbit with either a spectroscopic orbit or the parallax. We then choose the spectroscopic orbit that produces a total-mass estimate that agrees best with the parallax-based total mass. Finally, we calculate component masses from the ratio of the velocity amplitudes. Because the parallax constrains the total mass, the uncertainties of the component masses are considerably smaller than those obtained from the combination of the visual and spectroscopic orbits alone. The interferometry also produces a measurement of magnitude differences across the observed wavelength range.

As we show below, the component masses, luminosities, and colors present some problems for evolutionary models that have been applied to the Hyades. Determining the luminosities and the colors of the components is complicated by their rapid rotation. The recent discussion by Peterson et al. (2006) of the effects of rotation on Altair demonstrates that the observed colors and fluxes of a rapid rotator can differ significantly from those of an equivalent nonrotating star, depending on the inclination of the rotation axis to the line of sight. We have calculated corrections to $B - V$ and M_V based on the range of possible inclinations. Even with the range of possible corrections, problems with the evolutionary models remain.

We summarize the observational background for θ^2 Tau in § 2. We then describe the observations and analysis on which our visual orbit is based (§§ 3 and 4), present the resulting masses in § 5, and compare them with evolutionary models in § 6.

2. BACKGROUND

2.1. *Spectroscopic and Visual Orbits*

The binary nature of θ^2 Tau (= HR 1412 = HD 28319 = vB 72 = HIP 20894; α, δ [J2000.0] = $4^h28^m39^s.3$, 15°52′16″.4; $m_V = 3.41$; $B - V = 0.18$; Sp = A7 III [it is a standard for this spectroscopic type, despite its duplicity]) was first noted by Moore (1908) and Frost (1909). Plaskett (1915), Petrie (1940), and Ebbighausen (1959) measured the spectroscopic orbit of the primary but failed to detect the secondary, despite the fact that the magnitude difference is only slightly greater than 1 mag.

The secondary was first observed in lunar occultation observations (Evans & Edwards 1980; Peterson et al. 1981), and the difference Δv_R between the radial velocities of the components was measured at periastron using cross-correlation techniques by P91. The reason for the earlier lack of detection is the large rotational velocity of the secondary ($v_B \sin i$ is given variously between 90 and 170 km s^{-1}); its lines are broad and diffuse, and always blended with those of the primary.

The Mark III optical interferometer resolved the visual orbit in observations during 1989–1991, with preliminary results reported by Armstrong et al. (1991), Pan et al. (1992), and Hummel & Armstrong (1992). During the 1990s, three groups—PSL93, followed at 2 year intervals by TPM95 and TSL97—obtained spectroscopic data and combined the velocity amplitudes with the Pan et al. (1992) results to derive masses and the distance. However, the velocity amplitudes from the three groups are somewhat discordant, apparently due to their differing approaches to the line-blending problem. Their results—velocity amplitudes K, rotational velocities $v \sin i$, and mass ratios q—are summarized in the first half of Table 1.

PSL93 used synthetic spectra based on Kurucz (1991) model atmospheres to separate the contributions of the two components. They found a maximum cross-correlation between synthetic and observed spectra for $v_{A,B} \sin i = 65$ and 170 km s^{-1}, but the radial velocity of the secondary depended so sensitively on its rotational velocity that they could not derive a numerically stable value for its amplitude. Nevertheless, they were able to remove the effects of the secondary from the velocities of the primary. They then used velocity differences from P91 with the improved velocities of the primary to produce a spectroscopic orbit that included both components.

Unfortunately, the K_B results reported by PSL93 were in error because of a mistake in transcribing the Δv_R data from P91 (D. M. Peterson 1994, private communication). We have recalculated $K_{A,B}$ and q using velocities of the primary given by PSL93 and the Δv_R data of P91; these are the results that are shown in Table 1.

TPM95 cross-correlated their θ^2 Tau spectra with the spectra of radial velocity standards to get the velocity curve of the primary. They then subtracted the velocity-shifted spectrum of HR

[1] The Mark III optical interferometer, located on Mount Wilson, was jointly operated by the Naval Research Laboratory and the US Naval Observatory, with funding from the Office of Naval Research and from the Oceanographer of the Navy.
[2] The Navy Prototype Optical Interferometer is a joint project of the Naval Research Laboratory and the US Naval Observatory, in cooperation with Lowell Observatory.

1427, an A6 IV Hyades member with a projected rotational velocity approximately equal to that of θ^2 Tau A, from their data to produce spectra of θ^2 Tau B alone. From these spectra they obtained the velocity curve of the secondary and estimated that $v_B \sin i = 90$ km s^{-1} by comparison with the broadened spectrum of a sharp-lined star.

TSL97, like PSL93, compared their spectra to synthetic spectra. The synthetic spectra were composed of templates with $T_{\rm eff} = 8250$ K for both stars, $\log g = 4.0$ and 4.5 for the primary and secondary, respectively, and $v_A \sin i = 70$ km s^{-1}, with $v_B \sin i$ varying between 90 and 170 km s^{-1}. Because they were unable to obtain reliable secondary radial velocities from individual spectra, they took a global approach and found that $K_B = 38.0$ km s^{-1} and $v_B \sin i = 110$ km s^{-1} gave the best average correlation over all exposures.

The orbital parallaxes $\varpi_{\rm orb}$, distances D, and masses $\mathcal{M}$ derived by these three groups are summarized in the second half of Table 1 (with corrected results from PSL93). The distances are consistent within the uncertainties, as are the masses of the primaries. The secondary masses are slightly more discordant; the TPM95 and TSL97 ranges do not overlap, although the discrepancy is not large.

These distance and mass estimates have been cited by several authors. Narayan & Gould (1999) used θ^2 Tau with two other binaries to check for systematic errors in the *Hipparcos* parallaxes. Lastennet et al. (1999) used θ^2 Tau, also with two other binaries, to evaluate stellar evolution codes. Lebreton et al. (2001) used θ^2 Tau with four other binaries to construct an empirical mass-luminosity function and to assess the age and helium content of the cluster.

2.2. *Astrometry*

In 1997 the *Hipparcos* trigonometric parallaxes became available. For θ^2 Tau, $\varpi = 21.89 \pm 0.83$ mas (Perryman et al. 1997), as precise as the orbital parallaxes. Because the center of light moves over a range projected on the sky of $\approx$4.5 mas, the fact that the *Hipparcos* reduction treated θ^2 Tau as a single star is a possible reason for concern. It is likely, however, that the only effect is reduced precision, for several reasons. First, the residuals of the *Hipparcos* solution binned with the orbital period show only a very weak correlation with orbital phase, if any. Second, the orbital period is short compared to the length of the *Hipparcos* mission. Finally, the large eccentricity results in little motion of the center of light during most of the orbital period.

Dravins et al. (1997) used *Hipparcos* parallaxes and proper motions to determine the distance to the Hyades and parallaxes for its members, although they did not list individual parallaxes. They noted that the proper-motion-based parallaxes were about twice as precise as the trigonometric parallaxes. De Bruijne et al. (2001) used both *Hipparcos* and Tycho data to determine proper-motion parallaxes. For θ^2 Tau, they give a *Hipparcos* parallax of 22.24 ± 0.36 mas and a Tycho parallax of 22.35 ± 0.36 mas.

2.3. δ *Scuti Pulsations*

In a survey of Hyades A–F stars, Horan (1977, 1979) discovered that θ^2 Tau is a δ Scuti variable. The pulsations were confirmed, and more frequencies measured, by Breger et al. (1987, 1989); in addition, Breger et al. (1989) determined that it is the primary that is pulsating. New photometry by Breger et al. (2002) may show pulsations of the secondary as well. From the mass estimate published by TSL97, evolutionary modeling, and the observed pulsation frequencies, Breger et al. (2002) determined that θ^2 Tau A is close to the blue edge of the instability strip and that $T_{\rm eff} \lesssim 7800$ K. The lower mass estimate in our work moves θ^2 Tau A away from the edge of the strip, relaxing the constraint on $T_{\rm eff}$.

3. OBSERVATIONS AND CALIBRATION

We observed θ^2 Tau during 1989–1991 with the Mark III optical interferometer and obtained 30 nights of useful data, with between three and 42 scans per night in three spectral channels at 800, 550, and 450 nm in 1989, and at 800, 550, and 500 nm thereafter. Filter widths were 22 nm for 800 nm and 25 nm for the other wavelengths. The baseline lengths used varied between 8.2 and 31.5 m. A Mark III scan consisted of one 75 s stellar observation in three bands plus a 5 s background/dark count measurement. Descriptions of the Mark III in some detail are given by Shao et al. (1988) and Mozurkewich et al. (1991), and more briefly in the context of binary observations by, e.g., Armstrong et al. (1992).

We also observed θ^2 Tau in 1997 and 1998 with the NPOI and obtained four nights of useful data, with between four and seven scans per night in 19 spectral channels covering 850–520 nm. We used a configuration consisting of the center, east, and west astrometric stations, with baseline lengths of 37.5, 22.2, and 18.9 m. These scans consisted of one 90 s observation plus a 5 s background/dark count measurement. A description of the NPOI is given by Armstrong et al. (1998); binary observations with the NPOI are described by, e.g., Benson et al. (1997) and Hummel et al. (1998). The calibration of these data followed the methods we have used in previous work with Mark III and NPOI data, e.g., Mozurkewich et al. (1991) and Armstrong et al. (1992) for the Mark III, and Benson et al. (1997) and Hummel et al. (1998) for the NPOI.

The contributions of the two instruments to these results are about equal: 1052 visibilities in 30 nights from the Mark III, plus 785 visibilities and 122 closure phases in four nights from the NPOI. The separations from the four NPOI nights are in general more precise because of the greater number of visibilities per night. Table 2 lists the observations. The θ^2 Tau calibrated visibilities and closure phases, along with their uncertainties, are available in the electronic edition of the *Journal* in the FITS-based Optical Interferometry Data Exchange format (OIFITS) described by Pauls et al. (2005).[3]

4. DATA REDUCTION AND ANALYSIS

The data analysis method used here, described in detail by Hummel et al. (1993, 1998), consists of using the Marquardt-Levenberg method (e.g., Press et al. 1992) to fit a set of component parameters and orbital parameters directly to the entire set of measured visibilities $V^2(\lambda, t)$. The first θ^2 Tau results using this technique were reported by Hummel & Armstrong (1992). Fitting the parameters directly to the V^2 data, bypassing the stage of fitting (ρ, θ) values to each night's visibilities used by Armstrong et al. (1991) and Pan et al. (1992), allows us to use nights on which we took only a few scans and nights close to periastron during which the change in θ was not negligible. Fitting to the entire V^2 data set also gives us a more direct estimate of the parameter uncertainties.

The component parameters in the fit include the disk diameters $d_{A,B}$ and the magnitude difference parameterized by the differences at 500, 550, 700, and 800 nm. (Magnitude differences at other wavelengths were estimated by a spline interpolation.) The orbital parameters are the standard seven: the angular semimajor axis of the relative orbit a'', eccentricity e, period P, epoch of

[3] Defined at http://www.mrao.cam.ac.uk/~jsy1001/exchange.

TABLE 2
OBSERVATION AND RESULT LOG FOR θ^2 TAU

HJD (+2,440,000) (1)	Orbital Phase (2)	BL (m) (3)	Number of Scans (4)	ρ (mas) (5)	θ (deg) (6)	$\lvert O-C\rvert$ (mas) (7)	σ_{O-C} (mas) (8)
			1989 (Mark III)				
7772.967	0.195	31.5	6	21.24	7.88	0.17	0.30
7782.952	0.266	8.2	3	24.38	15.16	0.44	1.92
7790.961	0.323	23.1	4	26.02	23.62	1.02	0.97
7791.954	0.330	23.1	8	25.94	22.37	0.16	0.56
7804.952	0.422	31.5	8	26.34	28.88	0.51	0.54
7805.952	0.429	31.5	7	26.67	30.15	0.06	0.46
7806.947	0.436	31.5	7	27.44	33.32	1.39	1.10
7813.928	0.486	8.2	9	26.38	34.93	0.01	0.81
7818.933	0.521	15.2	6	26.18	38.83	0.46	0.43
7826.945	0.578	15.2	10	25.11	43.33	0.25	0.35
7827.966	0.585	15.2	6	25.45	44.61	0.82	1.26
7831.907	0.613	15.2	12	24.03	46.47	0.004	0.34
7832.911	0.621	27.0	20	24.03	47.62	0.26	0.13
7833.822	0.627	27.0	3	22.83	44.50	1.61	1.48
7836.827	0.648	23.3	13	23.22	50.74	0.30	0.32
7865.805	0.854	8.2	9	13.92	84.87	0.60	0.42
			1990 (Mark III)				
8148.966	2.866	15.4	8	14.14	88.52	0.23	0.12
8150.917	2.880	27.0	3	14.00	93.85	0.82	0.67
8187.803	3.142	23.6	7	17.77	359.06	0.45	0.57
8189.953	3.158	27.6	38	18.81	2.80	0.07	0.040
8192.922	3.179	31.5	42	20.23	6.12	0.03	0.11
8233.833	3.470	31.5	17	26.53	33.83	0.08	0.08
8234.827	3.477	31.5	20	26.49	34.39	0.07	0.17
			1991 (Mark III)				
8517.951	5.488	27.0	13	26.26	35.05	0.10	0.12
8548.927	5.709	15.2	18	20.86	57.32	0.14	0.14
8549.928	5.716	15.2	17	20.56	58.20	0.16	0.28
8562.911	5.808	15.2	15	17.08	73.88	0.30	0.23
8593.872	6.028	27.6	15	4.62	250.21	1.16	0.30
8594.793	6.034	27.6	12	4.69	274.87	0.88	0.22
8597.728	6.055	15.2	11	6.89	323.65	0.24	0.12
			1997 (NPOI)				
10459.722	19.286	37.5, 22.2, 18.9	6	24.93	18.29	0.06	0.067
10736.803	21.255	37.5, 22.2, 18.9	7	24.15	15.17	0.17	0.15
			1998 (NPOI)				
10836.680	21.965	37.5, 22.2, 18.9	7	8.92	134.44	0.14	0.034
11131.849	24.063	37.5, 22.2, 18.9	4	9.16	333.92	1.10	0.33

NOTES.—Col. (1): Heliocentric Julian Date of observation. Col. (2): Orbital phase relative to the epoch determined in this work and the period from TPM95. Col. (3): Baseline length(s). Col. (4): Number of scans available for that night. The orbital solutions used the fringe visibilities directly, rather than the intermediate solutions for each night's separation ρ and position angle θ; however, to indicate the quality of the data, the remaining columns give the results for fits to individual nights. Cols. (5) and (6): Best-fit separation ρ and position angle θ for each night. Col. (7): Distance from the best-fit position to the position predicted by the best-fit orbit. Col. (8): Distance from the best-fit position to the edge of the 68% confidence region, as measured along the $O-C$ vector.

periastron T, orbital inclination $i_{\rm orb}$, argument of periastron ω, and position angle of the line of nodes Ω.

In the case of θ^2 Tau, we did not fit for the component diameters $d_{\rm A,B}$. Instead, we estimated the diameters from the individual $R-I$ colors and apparent V magnitudes. We inferred the apparent magnitudes of the components from the system magnitude and the magnitude difference Δm from our data. As a starting point, we took the individual $R-I$ colors to be equal to the combined color (0.09 mag; Johnson et al. 1966) based on the observation that the colors of the components are nearly equal (Peterson et al. 1981; PSL93). We then applied the formulas given in Mozurkewich et al. (1991) and obtained uniform-disk diameter estimates at 800 nm of 0.76 and 0.42 mas. Because both angular diameters are below the resolutions of the Mark III and the NPOI configuration used (the smallest fringe spacing, at 520 nm on the 37.5 m NPOI baseline, was $\approx$2.8 mas), errors in the adopted diameters have a negligible effect on the estimates for other system parameters.

We adopted $P = 140.72816 \pm 0.00093$ days from TSL97, since it is based on observations spanning 90 years rather than the 9 years

covered by our observations. Then, with P and $d_{A,B}$ selected, we determined the other six orbital elements, redetermined Δm at four wavelengths, and repeated the orbit fitting after a slight adjustment of $d_{A,B}$. This procedure converged after one iteration.

The value of χ^2_ν at the best solution was 2.45. The most discrepant point in the orbit, in units of σ_{O-C}, is at JD 2,448,594.793 [$(\rho, \theta) = (4.69$ mas, $274\overset{\circ}{.}87)$]; when it is removed, χ^2_ν drops to 2.39 and the best solution shifts slightly. In the absence of a clear reason to exclude it, we have kept that night in the solution. (The point at JD 2,450,836.680 [$(\rho, \theta) = (8.92$ mas, $134\overset{\circ}{.}44)$] is more discrepant until the wavelength uncertainty of the NPOI, discussed below, is taken into account.)

We adopted the conservative assumption that χ^2_ν differs from unity due to underestimation of the observational uncertainties. Using increased observational uncertainties, we estimated the errors in the orbital elements from the curvature of the χ^2_ν hypersurface. We then checked these error estimates by confirming that perturbing the solution by 1 σ in one parameter and then fitting the remaining parameters produced an increase in χ^2_ν of one part in 1949, the number of degrees of freedom in the fit.

Our final step was to produce (ρ, θ) values and 68% confidence error ellipses for each night in order to illustrate the orbit. The distances from the nightly positions predicted by the best-fit orbit and those from the single-night fits are shown in column (7) of Table 2. Column (8) lists the distance from each single-night fit to the edge of the 68% confidence region, as measured along the line toward the predicted position for that night.

Included in the error estimate for the NPOI nights is a potential error in the angular scale due to the uncertainty in the wavelength scale. In the NPOI spectrometers, the dispersed light is focused on an array of lenslets that define the spectral channels. The lenslet arrays are aligned using the HeNe laser that is also used for aligning the beam-combiner table, delay lines, and feed system. The alignment is stable and accurate at the $\lesssim$0.5% level, which we adopt as our wavelength uncertainty for the NPOI data. Note that the Mark III used filters with well-measured and stable passbands and that the shift in $\lambda_{\rm eff}$ for the Mark III due to the spectral shape of an A star is less than one part in 3500.

Because the angular scale is proportional to $1/\lambda$, this uncertainty propagates directly into an uncertainty in the binary separation and in a''. The formal precision of a'' is very high: 18.796 $\pm$ 0.011 mas, or one part in 1700. Because about half of these data were taken with the Mark III, for which the wavelengths were well measured and stable, we adopt 0.3% as the uncertainty due to the wavelength scale. This value dominates the error budget and results in an uncertainty in a'' of 0.056 mas.

5. RESULTS AND DISCUSSION

The results of the visual orbit fitting are shown in Figure 1 and listed in Table 3, along with the elements from Armstrong et al. (1991), Pan et al. (1992), and Hummel & Armstrong (1992). Our orbit is consistent with the earlier, preliminary elements but has considerably higher precision, which we attribute to the method of directly fitting the V^2 data, the larger data set used, and improved coverage near periastron.

With the visual orbit in hand, determining the component masses proceeds in four steps. First, we determine the total mass of the system from a'', ϖ, and P, a result that is independent of $K_{A,B}$. Second, we determine the total mass implied by e, $i_{\rm orb}$, and the $K_{A,B}$ values of PSL93 (as corrected from P91), TPM95, or TSL97. These masses are independent of ϖ. Third, we choose the $K_{A,B}$ set that gives the best agreement with the first step. Finally, we divide the total mass between the components using q, the ratio of K_B to K_A.

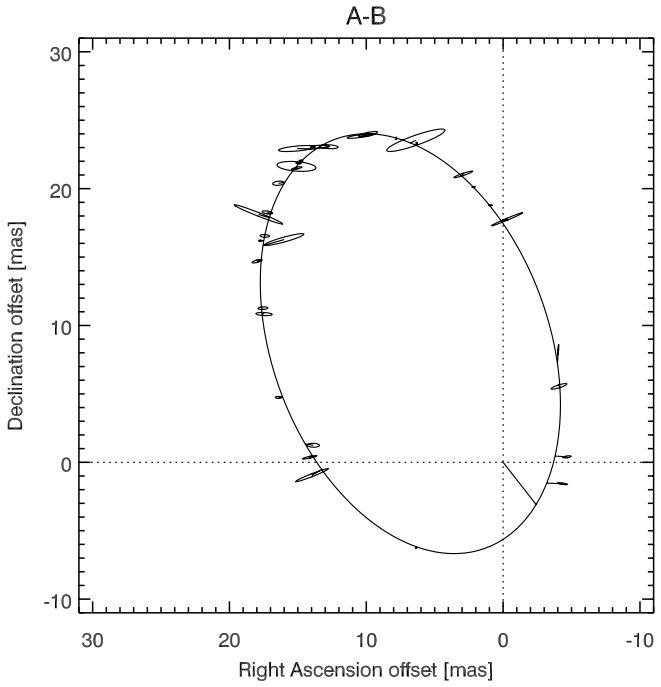

FIG. 1.—Visual orbit of θ^2 Tau. The ellipse shows the best-fit orbit as determined by a direct fit to the interferometric visibilities (see text). The center of each error ellipse marks the best-fit separation for one night's observations and is connected to the corresponding position on the best-fit orbit, while its size shows the 67% confidence region for that night's data. Some error ellipses are nearly too small to see in this figure, e.g., the point near $(\Delta\alpha, \Delta\delta) = (6.4, -6.2)$. The line from (0, 0) shows the position angle of periastron.

The total mass of the system, $\Sigma\mathcal{M}$, can be calculated directly from the parallax, the semimajor axis, and the period inserted into Kepler's third law:

$$\Sigma\mathcal{M}_{\varpi} = \mathcal{M}_A + \mathcal{M}_B = \frac{(a''/\varpi)^3}{P_{\rm yr}^2}\ \mathcal{M}_\odot, \qquad (1)$$

where the subscript ϖ indicates that the total mass is derived from the parallax and $P_{\rm yr}$ is of course the period in years. From Table 3 of de Bruijne et al. (2001), we adopt $\varpi = 22.30 \pm 0.36$ mas, the average of their parallaxes from the *Hipparcos* and the Tycho proper motions, which agree very well with one another. From our visual orbit, we adopt $a'' = 18.796 \pm 0.056$ mas, and from TSL97 we adopt $P_{\rm yr} = 0.38529$ yr with negligible uncertainty. The result is $\Sigma\mathcal{M}_{\varpi} = 4.03 \pm 0.20\ \mathcal{M}_\odot$, which appears in the first line of Table 4. The precision of this result, $\approx$6%, is dominated by the precision of ϖ.

As we discuss below, this $\Sigma\mathcal{M}_{\varpi}$ is smaller than the expected value, given the age and metallicity of the Hyades and the parallax and apparent magnitudes of θ^2 Tau. Note that using the Pan et al. (1992) value of 18.6 $\pm$ 0.2 mas for a'' gives an even smaller value, $3.91 \pm 0.25\ \mathcal{M}_\odot$, for $\Sigma\mathcal{M}_{\varpi}$. On the other hand, using the Perryman et al. (1997) *Hipparcos* trigonometric parallax with our a'' produces a larger value, $4.26 \pm 0.49\ \mathcal{M}_\odot$, with a considerably larger uncertainty.

We can also calculate the total mass from the velocity amplitudes $K_{A,B}$, eccentricity e, and orbital inclination $i_{\rm orb}$:

$$\Sigma\mathcal{M}_K = \mathcal{M}_A + \mathcal{M}_B = \frac{1.036\times10^{-7} P_d}{\sin^3 i_{\rm orb}}(K_A + K_B)^3\left(1-e^2\right)^{3/2}\ \mathcal{M}_\odot \qquad (2)$$

TABLE 3
VISUAL ORBITAL ELEMENTS FOR θ^2 TAU

Element	A91[a]	Pan92[b]	H92[c]	This Work
a (mas)	18.6	18.6 ± 0.2	18.7	18.796 ± 0.056
e	0.73	...	0.735	0.73725 ± 0.00036
P (days)	...	...	140.75	140.72816 (TSL97)
T − 2,440,000 (JD)	7748.2	...	7748.394	7748.576 ± 0.012
$i_{\rm orb}$ (deg)	46.7	46.2 ± 1.0	47.3	47.61 ± 0.09
ω (deg)	54	57.7 ± 1.7	54.8	55.40 ± 0.06
Ω (deg)	174.3	171.2 ± 1.8	174.2	173.73 ± 0.07
$\Delta m_{450\ {\rm nm}}$ (mag)	...	1.16 ± 0.13	1.0	...
$\Delta m_{500\ {\rm nm}}$ (mag)	...	...	...	1.05 ± 0.05
$\Delta m_{550\ {\rm nm}}$ (mag)	0.5	1.18 ± 0.10	1.0	1.12 ± 0.03
$\Delta m_{700\ {\rm nm}}$ (mag)	...	...	...	1.16 ± 0.03
$\Delta m_{800\ {\rm nm}}$ (mag)	...	1.15 ± 0.07	1.2	1.14 ± 0.05

[a] Armstrong et al. (1991).
[b] Pan et al. (1992).
[c] Hummel & Armstrong (1992).

(e.g., Heintz 1978, § 32), where the subscript K indicates that the sum is derived from the velocity amplitudes, P_d is the period in days, and $K_{\rm A,B}$ are in kilometers per second.

From the three sets of $K_{\rm A,B}$ and their uncertainties, combined with our values for $i_{\rm orb}$ and e and their uncertainties, plus the period of TSL97 once again, we calculated the three values for $\Sigma\mathcal{M}_K$ that are given in the last three lines of Table 4. These $\Sigma\mathcal{M}_K$ values differ from the sums of the masses in Table 1 from previous work because of the updated values for $i_{\rm orb}$ and e. The $\Sigma\mathcal{M}_K$ are less precise than $\Sigma\mathcal{M}_\varpi$ because of the difficulty in measuring the velocities in this system.

The best agreement between $\Sigma\mathcal{M}_K$ and $\Sigma\mathcal{M}_\varpi$ comes from using the TSL97 values for $K_{\rm A,B}$; values from PSL93/P91 and TPM95 give somewhat discrepant results. Therefore, we use q, the ratio of the velocity amplitudes from TSL97, to allocate $\Sigma\mathcal{M}$ between the components. We find $(\mathcal{M}_{\rm A}, \mathcal{M}_{\rm B}) = (2.15, 1.87)\ \mathcal{M}_\odot$.

The component masses are correlated, since they are constrained by $\Sigma\mathcal{M}$ and q. We calculated the joint probability $\mathcal{P}(\mathcal{M}_{\rm A}, \mathcal{M}_{\rm B})$ as a function of the two masses. In Figure 2 (*left*), we show the boundaries of the 50%, 68%, and 90% confidence regions in this joint $(\mathcal{M}_{\rm A}, \mathcal{M}_{\rm B})$ space. In particular, note that the highest total mass in the 68% confidence region is at $\mathcal{M}_{\rm A} = 2.31\ \mathcal{M}_\odot$, $\mathcal{M}_{\rm B} = 2.01\ \mathcal{M}_\odot$.

Our interferometric solution also includes the magnitude differences $\Delta m(\lambda)$, which are consistent with, but more precise than, the earlier results. In principle, calculating the components' absolute V magnitudes from the total m_V, Δm_V, and parallax is straightforward, yielding $(M_{V,\rm A},\ M_{V,\rm B}) = (0.48, 1.61)$ mag. The correlation between these magnitudes is shown in Figure 2 (*right*). The lowest luminosity extreme of the 68% confidence region lies at $M_{V,\rm A} = 0.54$ mag and $M_{V,\rm B} = 1.68$ mag. In practice, as we discuss toward the end of the next section, the rotation rate and inclination affect the apparent magnitude and color of each component, which complicates the comparison with evolutionary models. The component masses and magnitudes are summarized in Table 5.

TABLE 4
TOTAL MASS OF θ^2 TAURI

Parameter	$\Sigma\mathcal{M}$ $(\mathcal{M}_\odot)$
$\Sigma\mathcal{M}_\varpi$ (from visual orbit plus astrometry):	
a'' plus ϖ from de Bruijne et al. (2001)	4.03 ± 0.20
$\Sigma\mathcal{M}_K$ (from visual and spectroscopic orbits):	
e and $i_{\rm orb}$ plus $K_{\rm A,B}$ from P91/PSL93	4.50 ± 0.47
e and $i_{\rm orb}$ plus $K_{\rm A,B}$ from TPM95	3.40 ± 0.43
e and $i_{\rm orb}$ plus $K_{\rm A,B}$ from TSL97	4.02 ± 0.35

6. COMPARISON WITH EVOLUTIONARY MODELS

6.1. *Observed Magnitudes and Colors*

The masses and absolute magnitudes we derive here pose a problem in the context of some recent sets of isochrones. If we accept the current estimates of the helium content ($Y \approx 0.28$) and metallicity (the spectroscopic [Fe/H] is ≈0.14, or $Z \approx 0.026$) of the Hyades, an age t of roughly 600 Myr does the least violence to the masses and absolute V magnitudes that we derive. However, even isochrones near this age result in stars whose masses are too small for their luminosities. For stars of 2.31 and 2.01 $\mathcal{M}_\odot$, these magnitudes are somewhat brighter than those expected from evolutionary models fit to other Hyades binaries. The disagreement may not be surprising in view of the difficulties in modeling near the main-sequence turnoff.

For instance, the point where the $Y = 0.28$, $Z = 0.026$, $t = 700$ Myr isochrone of Lebreton et al. (2001) passes through the color and magnitude of the secondary, $B - V = 0.18$ mag, $M_V = 1.61$ mag, corresponds to a mass of 1.98 $\mathcal{M}_\odot$, just within our 68% confidence contour. But this isochrone does not pass near the point $B - V = 0.18$ mag, $M_V = 0.48$ mag that corresponds to the primary of θ^2 Tau. At $B - V = 0.18$ mag, this isochrone has $\mathcal{M} = 2.28\ \mathcal{M}_\odot$, an acceptable mass, but it is too faint at $M_V = 0.8$ mag. On the other hand, if we boost the luminosity to set $M_V = 0.49$ mag (the nearest tabulated point), the isochrone has the component as too massive ($\mathcal{M} = 2.41\ \mathcal{M}_\odot$) and too red ($B - V = 0.26$ mag). Older isochrones are too red to match the secondary.

The $Y = 0.30$, $Z = 0.030$, $t = 560$ Myr isochrone of Girardi et al. (2000) fares slightly better, as illustrated in Figure 3. It passes through the color and magnitude of the secondary at a mass of 2.00 $\mathcal{M}_\odot$, and through the color and magnitude of the primary at a mass of 2.44 $\mathcal{M}_\odot$. This pair of masses is just beyond the 90% confidence contour. The isochrones of Lejeune & Schaerer (2001) and the empirically adjusted Hyades isochrone of Pinsonneault et al. (2004) show similar results. (In Fig. 3*a*, the more heavily marked parts of the isochrones correspond to

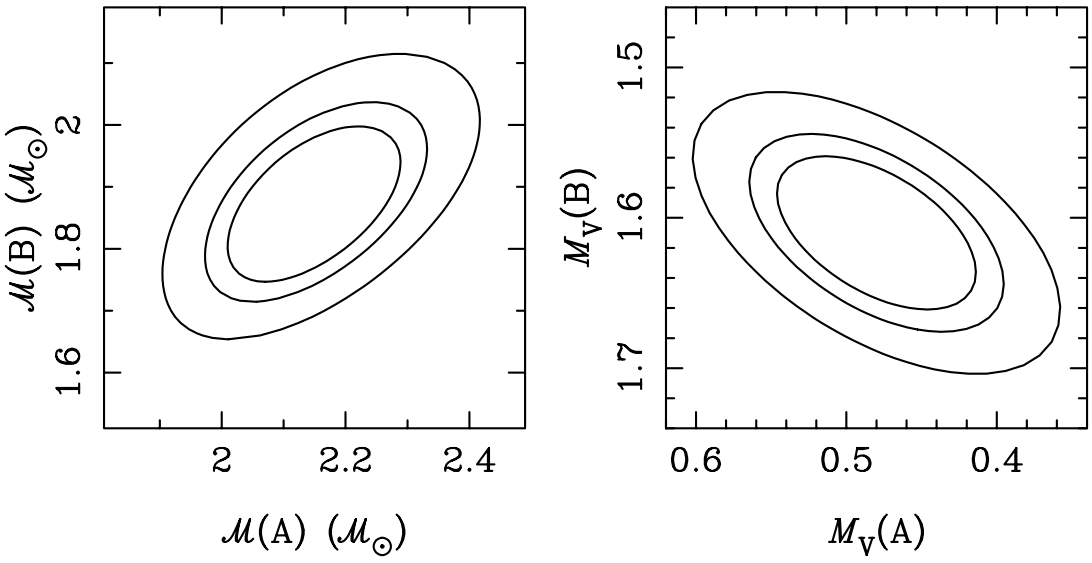

FIG. 2.—Confidence contours of the component masses (*left*) and absolute V magnitudes (*right*) of θ^2 Tau. Contour levels are for the 50%, 68%, and 90% confidence regions.

the 1 σ ranges of allowed masses for the two components, and the points corresponding to the best-fit masses are marked with filled circles.)

The agreement between the isochrones and our results would be considerably better if Z took the solar value of 0.019, although this value would not fit the rest of the Hyades. The gray line in each panel of Figure 3 is an isochrone at $t = 750$ Myr, $Z = 0.019$, interpolated between the 710 and 790 Myr isochrones of Girardi et al. (2000). The observed θ^2 Tau B color and magnitude fit this isochrone well along a stretch of the isochrone that also corresponds to the correct mass within its uncertainties. This isochrone passes through the θ^2 Tau A color and magnitude within their uncertainties, but at the wrong mass. However, the error bar in Figure 3*b* shows that the mass discrepancy for component A is barely more than 1 σ. An isochrone of Lejeune & Schaerer (2001) with $t = 790$ Myr and solar metallicity is similarly close to the best-fit values of color, magnitude, and mass.

The situation is somewhat unsatisfactory: the isochrones that fit are only a little older than current estimates, but they are significantly metal-poor for a member of the Hyades. To get metal-rich isochrones that agree with our results, one would have to increase the helium content significantly, which is at odds with the constraints placed on Y by the low-mass Hyades double-lined eclipsing binary vB 22 by Lebreton et al. (2001), 0.255 $\pm$ 0.006, and Pinsonneault et al. (2003), 0.271 $\pm$ 0.006, both less than the solar-scaled value of 0.28.

6.2. *Effects of Rotation*

Can the discrepancies be resolved by invoking the effects of stellar rotation on the observed colors and magnitudes, discussed in the context of Altair by Peterson et al. (2006)? Our results

TABLE 5
COMPONENT MASSES AND ABSOLUTE MAGNITUDES

Parameter	A	B
Mass ($\mathcal{M}_\odot$)	2.15 $\pm$ 0.12	1.87 $\pm$ 0.11
M_V (mag)	0.48 $\pm$ 0.05	1.61 $\pm$ 0.06

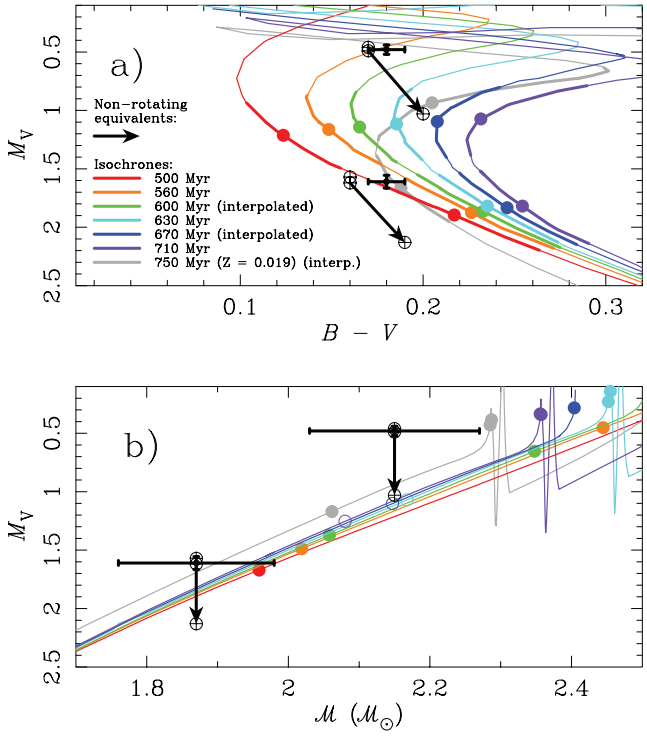

FIG. 3.—Components of θ^2 Tau compared to Girardi et al. (2000) isochrones with $Y = 0.30$. For the colored isochrones, $Z = 0.03$. An isochrone with $Z = 0.019$, in gray, is shown for comparison. (*a*) Color-magnitude diagram. The thicker portions of the isochrones mark the ± 1 σ mass ranges. The best-fit masses are marked by filled circles. Crossed black error bars mark the observed $B - V$ and M_V for each component. Open circles with crosses show the locations of nonrotating stars of the same mass and luminosity, for three inclination angles. In the order shown by the arrows, $i = 90°$ (equator-on), $i = 47.°6$ ($=i_{\rm orb}$), and $i = 13.°5$ (rotation at breakup velocity) for the primary; and $i = 90°$, $47.°6$, and $17.°3$ for the secondary (using $v \sin i = 110$ km s^{-1}). (*b*) Mass-magnitude diagram. Isochrones are color coded as in (*a*). Filled circles mark where $B - V = 0.18$ mag (with no correction for rotation). On the 630–710 Myr isochrones, the bluest points before the turnoff ($B - V = 0.184$, 0.21, and 0.22 mag, respectively) are marked with open circles. Crossed black error bars show the observed masses and M_V. Open circles with crosses show the locations of the nonrotating equivalents, in the same order as in (*a*).

TABLE 6
EFFECTS OF ROTATION

Inclination (deg) (1)	Rotating Star T_{polar} (K) (2)	Rotating Star v_{eq} (km s^{-1}) (3)	Rotating Star ω (4)	Nonrotating Equivalent M_V (5)	Nonrotating Equivalent $B-V$ (6)	Nonrotating Equivalent T_{eff} (K) (7)
Primary ($\mathcal{M}$ = 215 $\mathcal{M}_\odot$, $v \sin i$ = 65 km s^{-1})						
90	7957	65	0.35	0.46	0.17	7915
47.6 (=i_{orb})	7988	89	0.47	0.49	0.17	7910
13.5	8748	300	0.999	1.03	0.20	7820
Secondary ($\mathcal{M}$ = 187 $\mathcal{M}_\odot$, $v \sin i$ = 110 km s^{-1})						
90	8291	110	0.47	1.57	0.16	8205
47.6 (=i_{orb})	8396	149	0.561	1.62	0.16	8230
17.3	9039	370	0.999	2.13	0.19	8080

NOTES.—Col. (1): Assumed inclination for each case. Cols. (2) and (3): Derived polar effective temperature and rotational velocity for the observed star with the given inclination. Col. (4): Rotational velocity of the star as a fraction of breakup velocity. Cols. (5)–(7): Absolute V magnitude, $B-V$ color, and effective temperature for the equivalent nonrotating star of the same mass.

show that rotation does not alter the appearances of the components in a way that resolves these discrepancies.

Rapid rotation has several effects. For stars in this mass range, the luminosity and polar radius decrease slightly (e.g., Sackmann 1970) while the equatorial radius increases significantly, reaching 3/2 the polar radius at breakup angular velocity (Hardorp & Strittmatter 1968). The effective temperature of the equatorial region decreases significantly; in the case of Altair, an A star with a mass of 1.8 $\mathcal{M}_\odot$ and rotating at 90% of breakup velocity, the pole-to-equator temperature difference is 1850 K (Peterson et al. 2006).

Thus, a rotating star does not radiate isotropically (Kraft 1970). Because of the variation in intensity across the surface, a star rotating near breakup velocity and seen nearly pole-on appears significantly brighter than it would if it were not rotating, in spite of the slight reduction in total luminosity. A star with the same $v \sin i$ but rotating equator-on has a smaller rotational velocity; thus, its luminosity is only slightly reduced and the pole-to-equator variation is less. The net effect in this case is that the star appears slightly fainter and somewhat redder than the nonrotating equivalent, since our view of the star is dominated by the cooler equatorial regions. Figueras & Blasi (1998) have shown that the ages of open clusters derived from upper-main-sequence isochrone fitting can be overestimated by 30%–50% if the effects of rotation on *ubvy*Hβ colors are not accounted for.

We used the suite of programs developed by Peterson et al. (2006) to calculate the run of specific intensity across the surface of a Roche spheroid and the resulting appearance of such a star as seen from a specific direction. The models were computed at the masses determined in this work and were constrained to reproduce the observed V magnitude, $B-V$ color, and $v \sin i$. They were calculated for three inclination angles for each of the binary components: at the minimum possible inclination, i.e., the inclination that implies that the star is rotating at breakup angular velocity; at $i = i_{orb}$; and at $i = 90^\circ$, i.e., equator-on.

Figure 3 shows the results of our calculations as open circles with crosses: the upper three points for the primary at 2.15 $\mathcal{M}_\odot$ and the lower three for the secondary at 1.87 $\mathcal{M}_\odot$. Each point shows the absolute V magnitude and the $B-V$ color of the nonrotating equivalent star of the appropriate mass that, if it were rotating, would match the observed values of V, $B-V$, and $v \sin i$. The $i = 90^\circ$ and $i = i_{orb}$ cases produce nearly identical values for M_V and $B-V$ for the nonrotating equivalents, while for the minimum inclination, indicated by the arrow, the nonrotating equivalent stars are considerably fainter and somewhat redder. The results are also summarized in Table 6.

The results of these calculations do not substantially improve the agreement between our observations and the evolutionary models. To demonstrate this point, we replot in Figure 4 the models shown in Figure 3, but as evolutionary tracks for $\mathcal{M}$ = 2.27, 2.15, and 2.03 $\mathcal{M}_\odot$ (the best-fit mass [$\pm\sigma_{\mathcal{M}}$]) for the primary, and for $\mathcal{M}$ = 1.98, 1.87, and 1.76 $\mathcal{M}_\odot$ for the secondary. The nonrotating equivalents—calculated at 2.15 and 1.87 $\mathcal{M}_\odot$—are repeated from Figure 3 as well.

For the primary, the 2.15 $\mathcal{M}_\odot$ nonrotating equivalent falls near the 2.15 $\mathcal{M}_\odot$ evolutionary track near an age of 670 Myr, but only if the primary itself is rotating at breakup velocity. For the secondary, the situation is worse: the 1.87 $\mathcal{M}_\odot$ nonrotating equivalent crosses the 1.87 $\mathcal{M}_\odot$ track considerably blueward of the 500 Myr point, the youngest one plotted, and then only if the secondary itself is rotating close to breakup velocity.

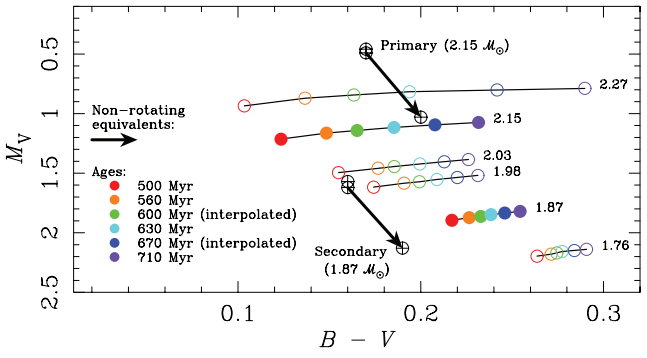

FIG. 4.—Nonrotating equivalents of the components of θ^2 Tau compared to evolutionary tracks from Girardi et al. (2000) with $Y = 0.30$. Tracks are plotted for stars with masses equal to those of the primary and secondary, $\pm\sigma_{\mathcal{M}}$. The colors and magnitudes of the 2.15 and 1.87 $\mathcal{M}_\odot$ nonrotating equivalents, i.e., nonrotating stars that, were they rotating, would produce the observed V, $B-V$, and $v \sin i$, are also plotted.

7. SUMMARY

We have measured the visual orbit of the spectroscopic binary θ^2 Tauri with the Mark III optical interferometer and the Navy Prototype Optical Interferometer. The results, combined with other data in the literature, allow us to determine the masses and absolute magnitudes of the components and to test some of the current stellar evolution results.

We used our measurement of the angular size of the orbit in conjunction with the parallax of de Bruijne et al. (2001) and the orbital period of Torres et al. (1997) to calculate the total mass of the system by way of Kepler's third law. In order to choose among the three spectroscopic orbits in the literature, we used each of them to estimate the total mass and chose the one (Torres et al. 1997) that agreed best with the parallax result. We then used the ratio of velocity amplitudes to allocate the total mass between the two components.

The resulting masses are 1.87 ± 0.11 and 2.15 ± 0.12 $\mathcal{M}_\odot$ considered individually; considered jointly, masses of 2.01 and 2.31 $\mathcal{M}_\odot$ lie just within the 68% confidence contour. The absolute V magnitudes are 0.48 and 1.61 mag. The estimated masses, especially the mass of the primary, are somewhat small compared to those implied by the observed absolute magnitudes and evolutionary models for the age and metallicity of the Hyades. We also calculated the possible effects of rotation on the magnitudes and colors of the components. The results do not reconcile the measured masses with the evolutionary models.

We thank Lu Rarogiewicz for years of unfaltering assistance in operating the Mark III interferometer, Craig Denison for even more years of careful and conscientious assistance with both the Mark III and the NPOI, and H. R. Schmitt, R. T. Zavala, B. D. Mason, and H. C. Harris for careful reading of the manuscript. This work was funded by the Office of Naval Research and the Oceanographer of the Navy. We have made use of the SIMBAD database operated by the CDS, Strasbourg, France, and of NASA's Astrophysics Data System.

REFERENCES

Armstrong, J. T., Hummel, C. A., & Mozurkewich, D. 1991, in High-Resolution Imaging by Interferometry II, ed. J. M. Beckers & F. Merkle (Garching: ESO), 673
Armstrong, J. T., et al. 1992, AJ, 104, 241
———. 1998, ApJ, 496, 550
Benson, J. A., et al. 1997, AJ, 114, 1221
Breger, M., Garrido, R., Lin, H., Shi-yang, J., Zi-he, G., Fruch, M., & Paparo, M. 1989, A&A, 214, 209
Breger, M., Lin, H., Shi-yang, J., Zi-he, G., Antonello, F., & Mantegazza, L. 1987, A&A, 175, 117
Breger, M., Pamyatnykh, A. A., Zina, W., Garrido, R., Handler, G., & Reegen, P. 2002, MNRAS, 336, 249
de Bruijne, J. H. J., Hoogerwerf, R., & de Zeeuw, P. T. 2001, A&A, 367, 111
Dravins, D., Lindegren, L., Madsen, S., & Holmberg, J. 1997, in *Hipparcos*, Venice '97, ed. B. Battrick (ESA SP-402; Noordwijk: ESA), 733
Ebbighausen, E. G. 1959, Publ. Dom. Astrophys. Obs., 11, 235
Evans, D. S., & Edwards, D. A. 1980, Observatory, 100, 206
Figueras, F., & Blasi, F. 1998, A&A, 329, 957
Frost, E. B. 1909, ApJ, 29, 233
Girardi, L., Bressan, A., Bertelli, G., & Chiosi, C. 2000, A&AS, 141, 371
Hardorp, J., & Strittmatter, P. A. 1968, ApJ, 151, 1057
Heintz, W. D. 1978, Double Stars (Dordrecht: Reidel)
Horan, S. 1977, Bull. Inf. Var. Stars, 1232, 1
———. 1979, AJ, 84, 1770
Hummel, C. A., & Armstrong, J. T. 1992, in IAU Colloq. 135, Complementary Approaches to Double and Multiple Star Research, ed. H. A. McAlister & W. I. Hartkopf (ASP Conf. Ser. 32; San Francisco: ASP), 552
Hummel, C. A., Armstrong, J. T., Quirrenbach, A., Buscher, D. F., Mozurkewich, D., Simon, R. S., & Johnston, K. J. 1993, AJ, 106, 2486
Hummel, C. A., Mozurkewich, D., Armstrong, J. T., Hajian, A. R., Elias, N. M., II, & Hutter, D. J. 1998, AJ, 116, 2536
Johnson, H. L., Iriarte, B., Mitchell, R. I., & Wisniewski, W. Z. 1966, Comm. Lunar Planet. Lab., 4, 99
Kraft, R. P. 1970, in Spectroscopic Astrophysics, ed. G. H. Herbig (Berkeley: Univ. California Press), 385
Kurucz, R. L. 1991, in Precision Photometry: Astrophysics of the Galaxy, ed. A. G. D. Philip, A. R. Upgren, & K. A. Janes (Schenectady: Davis), 27
Lastennet, E., Valls-Gabaud, D., Lejeune, Th., & Oblak, E. 1999, A&A, 349, 485
Lebreton, Y., Fernandes, J., & Lejeune, Th. 2001, A&A, 374, 540
Lejeune, Th., & Schaerer, D. 2001, A&A, 366, 538
Moore, J. H. 1908, Lick Obs. Bull., No. 146
Mozurkewich, D., Johnston, K. J., Simon, R. S., Bowers, P. F., Gaume, R. A., Hutter, D. J., Colavita, M. M., & Shao, M. 1991, AJ, 101, 2207
Narayan, Y. K., & Gould, A. 1999, ApJ, 515, 256
Pan, X.-P., Shao, M., & Colavita, M. M. 1992, in IAU Colloq. 135, Complementary Approaches to Double and Multiple Star Research, ed. H. A. McAlister & W. I. Hartkopf (ASP Conf. Ser. 32; San Francisco: ASP), 502
Pauls, T. A., Young, J. S., Cotton, W. D., & Monnier, J. D. 2005, PASP, 117, 1255
Perryman, M. A. C., et al. 1997, The *Hipparcos* and Tycho Catalogues (ESA SP-1200; Noordwijk: ESA)
———. 1998, A&A, 331, 81
Peterson, D. M. 1991, in ASP Conf. Ser. 13, The Formation and Evolution of Star Clusters, ed. K. A. Janes (San Francisco: ASP), 592 (P91)
Peterson, D. M., Baron, R. L., Dunham, E., & Mink, D. 1981, AJ, 86, 1090
Peterson, D. M., Stefanik, R. P., & Latham, D. W. 1993, AJ, 105, 2260 (PSL93)
Peterson, D. M., et al. 2006, ApJ, 636, 1087
Petrie, R. M. 1940, PASP, 52, 286
Pinsonneault, M. H., Terndrup, D. M., Hanson, R. B., & Stauffer, J. R. 2003, ApJ, 598, 588
———. 2004, ApJ, 600, 946
Plaskett, J. S. 1915, Publ. Dom. Astrophys. Obs., 2, 63
Press, W. H., Flannery, B. P., Teukolsky, S. A., & Vetterling, W. T. 1992, Numerical Recipes in C (2nd ed.; Cambridge: Cambridge Univ. Press)
Sackmann, I.-J. 1970, A&A, 8, 76
Shao, M., et al. 1988, A&A, 193, 357
Tomkin, J., Pan, X.-P., & McCarthy, J. K. 1995, AJ, 109, 780 (TPM95)
Torres, G., Stefanik, R. P., & Latham, D. W. 1997, ApJ, 485, 167 (TSL97)